Microcantilever dynamics in liquid environment dynamic atomic force microscopy when using higher-order cantilever eigenmodes

Daniel Kiracofe and Arvind Raman[a)]
School of Mechanical Engineering and Birck Nanotechnology Center, Purdue University, West Lafayette, Indiana 47904, USA

(Received 5 April 2010; accepted 27 May 2010; published online 10 August 2010)

Dynamic atomic force microscopy is currently evolving from a single to a multifrequency instrument for nanoscale imaging often employing higher-order microcantilever eigenmodes for improved resolution and force spectroscopy. In this work the authors study the fundamentals of cantilever dynamics and energy dissipation when soft cantilevers are driven at their second flexural eigenmode and interact with samples in liquid environments. Contrary to the conventional first eigenmode operation, second eigenmode operation in liquids is often dominated by a subharmonic response (e.g., one tap every four drive cycles) and there is an energy transfer to the first eigenmode creating a new channel of energy dissipation and compositional contrast. © *2010 American Institute of Physics*. [doi:10.1063/1.3457143]

Many newer dynamic atomic force microscopy (dAFM) methods aim to excite higher-order eigenmodes of the microcantilevers in liquid environments for improved resolution or compositional contrast on biological samples under physiological native conditions or for studies of ordered water on solid-liquid interfaces. For example, because the stiffness and quality factor of the second eigenmode is higher than that of the fundamental, stable imaging may be possible at smaller oscillation amplitudes,[1] the phase contrast may be better,[2] and for some situations the undesirable "forest of peaks" in acoustic drive[3] may be reduced. In addition, the second eigenmode is also driven as a part of "dual-ac" or bimodal schemes[4] for increased compositional contrast.

Yet, before moving to these excitation schemes it is important to understand how, if at all, operating at eigenmodes beyond the fundamental is different from operating at the fundamental eigenmode. In this work, the dynamics of AFM cantilevers in liquids are investigated when the cantilever is driven at its second natural frequency; a situation which, from prior work in air or vacuum, ought not be essentially different from operating at the fundamental natural frequency. The dynamics in fact can be surprisingly different-often showing an unexpected strong, $1/n$ subharmonic response that leads to the excitation of the first eigenmode, causing the tip to tap on the sample in a period n pattern that repeats every n drive cycles. This finding has major implications for the use of second and other higher-order eigenmodes in liquid environment AFM for imaging, compositional contrast, and force spectroscopy.

The experimental method is as follows. An Agilent 5500 AFM with acoustic drive[23] is used. Results are initially presented for Mikromasch CSC37B cantilevers and results for other levers are discussed later. The driving frequency was chosen as the acoustic tuning peak closest to *thermal tune peak of the second eigenmode*. The magnitudes of the subharmonics were monitored using additional lock-ins. Experimental approach curves were repeated over one hundred times (including different cantilevers and different areas of the substrate) and were quite repeatable.

The samples studied were freshly cleaved mica and purple membrane (PM). The PM was wild-type bacteriorhodopsin isolated from *Halobacterium salinarum* (Sigma-Aldrich). The PM was deposited on mica and incubated for 15 min. Then the buffer solution was wicked off and the liquid cell was filled with fresh buffer (20 mM TrisCl 300 mM KCl).

The VEDA simulator (Ref. 5) was used to mathematically simulate the cantilever dynamics in liquids when the second eigenmode is driven and the cantilever interacts with the sample. A three eigenmode model [Fig. 1(a)] is used.[24] The equations of motion are[6]

$$\frac{\ddot{q}_i}{\omega_i^2}+\frac{\dot{q}_i}{\omega_i Q_i}+q_i=\frac{F_{ts}(d)}{k_i}+\frac{F_i\cos\Omega_d t}{k_i},\quad i=1,\ldots,3,$$

where $q_i(t)$, ω_i, Q_i, k_i, F_{ts}, and F_i are the tip deflection (relative to base motion[3,7]), natural frequency, quality factor, equivalent stiffness, tip-sample interaction force, and driving force of the ith eigenmode, respectively, Ω_d is the driving frequency ($\Omega_d \approx \omega_2$ for this work), $d=Z+y+\Sigma_{i=1}^{3}q_i$ is the tip-sample gap, where Z is the cantilever-sample separation and $y(t)$ is the motion of the cantilever base due to dither piezoexcitation. For simplicity, a Hertz contact model is used to describe the tip-sample interaction force:[25]

$$F_{ts}(d)=\begin{cases}0, & d>0\\ \frac{4}{3}E^*\sqrt{R}(-d)^{3/2}, & d\le 0\end{cases},$$

where R is the tip radius and E^* is the reduced elasticity $E^*=[(1-\nu_{\text{tip}}^2)/E_{\text{tip}}+(1-\nu_{\text{sample}}^2)/E_{\text{sample}}]^{-1}$ where ν and E are Poisson's ratio and Young's modulus.

Because the optical lever scheme in most AFMs measures slope not actual deflection, the observed deflection is $u=\Sigma_{i=1}^{3}\chi_i q_i$, where χ_i is the slope at the end of the cantilever

[a)]Electronic mail: raman@ecn.purdue.edu.

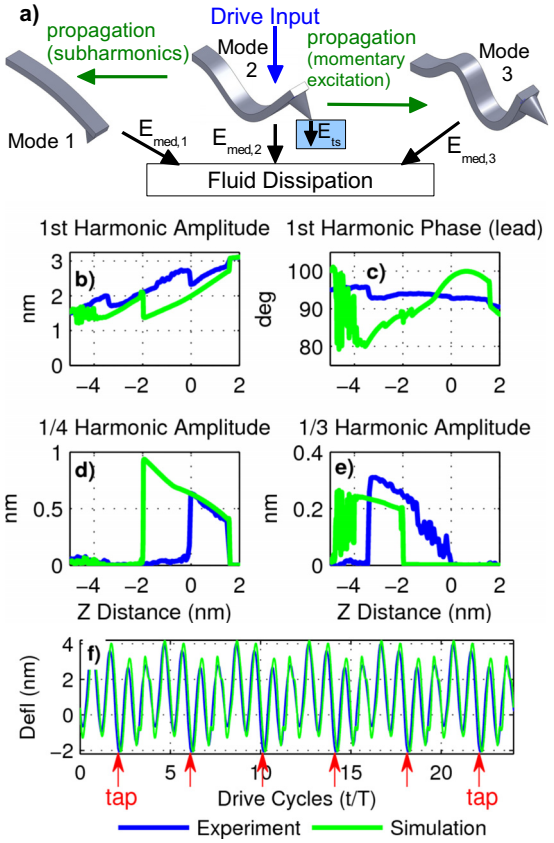

FIG. 1. (Color online) (a) Schematic of the three eigenmodes used and the energy flow between them. (b)–(e) Simulated vs experimental approach curves on mica in buffer solution. Amplitudes are nm peak observed deflection calibrated to second eigenmode. (f) Time history of experimental and simulation deflection at $Z=1$ nm.

in the ith eigenmode. For a uniform rectangular beam $\chi_2/\chi_1=3.47$, $\chi_3/\chi_1=5.70$. In this paper we report the experimentally observed tip deflection by multiplying the observed photodiode signal (volt) by $(1/\chi_2)*$sensitivity (nanometer per volt) of the first eigenmode. When the cantilever is not contacting the surface the response is dominated by the second eigenmode and observed tip deflection equals actual deflection. However, in intermittent contact other eigenmodes are excited so observed deflection is some combination of the different eigenmodes but the contribution of each eigenmode is unknown so it is impossible to know the actual tip motion. Thus the sensitivity calibration provides only an estimate of the amplitude.

The parameters used in the simulations are given in Table I and are based on a typical Mikromasch CSC37B cantilever. The tip radius has been tuned to match the experimental results. No other parameters have been tuned.

Figure 1 shows experimental and simulated approach curves on mica in buffer solution. Figure 1(b) plots the first harmonic (i.e., at driving frequency) amplitude. Rather surprisingly, the amplitude is nonmonotonic with Z. Similar jumps between attractive and repulsive regimes are well known,[8] but the simulation uses a Hertz contact model that has no attractive forces so that cannot be the cause in this case. Figures 1(d) and 1(e), which plot the amplitudes of different subharmonics, give a clue to this phenomenon. The jump downs in the first harmonic amplitude correspond to

TABLE I. Simulation parameters (typical of experimental parameters).

Natural frequency (kHz)	10, 76, 212
Driving frequency (kHz)	76
Modal stiffness (N/m)	0.6, 23.6, 185
Unconstrained amplitude (nm)	3.1
Quality factor $(\frac{1}{2\zeta})$	2.8, 6.5, 9
Tip radius (nm)	2
Tip Young's modulus (GPa)	130
Poisson's ratio	0.3
Sample Young's modulus (GPa)	60
Approach speed (nm/s)	20
Lock-in bandwidth (kHz)	2

jump ups in the 1/4 and 1/3 harmonic amplitude indicating the onset of subharmonic response. Subharmonic behavior in AFM has been studied before,[9–16] however, the majority of the studies are limited to driving frequencies near the first natural frequency and all are restricted to ambient air or nitrogen environments.

The exact nature of the subharmonic response is best understood in terms of a time history plot. Figure 1(f) shows the simulated and experimental[26] time histories of observed deflection near $Z=1$ nm. The tip does not tap on the sample every drive cycle, rather, there is a pattern that repeats once every four drive cycles. This is a period 4 response, which corresponds to a significant cantilever response at 1/4 the drive frequency. In essence, when the tip taps on the sample, the sudden impact transfers energy from the driven harmonic to both higher and lower frequencies (i.e., the first and third eigenmode)[17] as shown in Fig. 1(a). The response of the first eigenmode causes the tip to rebound off the sample so far that it does not tap the sample on the next drive cycle and a subharmonic motion is created.

For stiff samples, this subharmonic response can be understood from the theory of a vibroimpact oscillator that is driven above its natural frequency ω_1 (Ref. 18) where it is known that when the drive frequency $\Omega_d \approx 2n\omega_1$ then the oscillator can strongly respond at the frequency Ω_d/n. That is, subharmonics solutions can occur when the forcing executes (approximately) an integer number of cycles while the first eigenmode executes a half cycle. For the cantilever used in Fig. 1, an initial period 4 solution is consistent with the prediction for the drive frequency $\Omega_d/\omega_1=7.6$. The transition to period 3 response may reflect the increase in the nonlinear natural frequency of the first eigenmode due to tip-sample interactions. For softer samples, the impact oscillator limit does not apply and a more detailed analysis would be necessary.

dAFM experiments are performed in a variety of settings therefore it is important to understand the range of physical parameters for which subharmonic response is likely to occur in experiments. The two most important factors are the ratio of effective sample stiffness to cantilever stiffness $[\bar{k}=(E^*\sqrt{A_{\text{initial}}R})/k_1]$ and the damping (Q_i) of the eigenmodes. The effects of these factors are studied in Fig. 2. Several hundred approach curves were simulated for various values of Q_1 and k_1, keeping the ratios of k_i/k_1 and Q_i/Q_1 constant $(i=2,3)$. The remaining parameters were as in Fig. 1 except

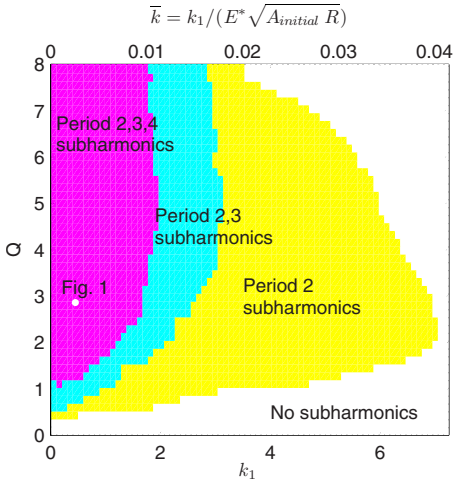

FIG. 2. (Color online) Map of subharmonic regions for a range of k_1 and Q_1. The ratios k_i/k_1 and Q_i/Q_1 were kept constant ($i=2,3$). Approach curves were run to 20% setpoint ratio. The simulation of Fig. 1 is marked. The other parameters are the same as Table I except $A_{\text{initial}}=1.5$ nm.

$A_{\text{intital}}=1.5$ nm. The upper x-axis plots the nondimensional stiffness ratio $\bar{k}$ from which conclusions about the effect of sample stiffness and initial amplitude can be drawn. Each approach curve was examined to determine what types of subharmonics occurred (1/4, 1/3, 1/2, or none). From this the map is divided into four regions.

From Fig. 2 the effect of stiffness is obvious: if the cantilever stiffness is increased (or equivalently, if the sample modulus or initial amplitude decreased), then the subharmonic response will decrease and eventually disappear. The effect of damping on the subharmonic response is more complex, however very low Q factors tend to suppress the subharmonic response.

As an example of this, the experiments were repeated using the following cantilevers with two different tip heights: Mikromasch cantilevers that have >20 μm tip height (CSC36B, CSC37B, CSC37C, and CSC38B) and Olympus cantilevers that have <3 μm tip height (RC800PSA, RC150VB, TR400PB). The subharmonic behavior occurred for all Mikromasch cantilevers tested but did not occur for any Olympus cantilever tested. This is because the Olympus cantilevers' short tip height causes a large amount of squeeze-film damping,[19] making the first eigenmode highly damped (in fact $Q_1<1$ when within imaging distance of the sample).

The subharmonic responses are also sensitive to the presence of tip debris. In the experiments, a new cantilever on clean mica would always demonstrate period 4 subharmonics. However, after scanning a biological sample, the period 4 subharmonics often disappeared but period 3 or 2 subharmonics persisted. Presumably, as the tip picks up small amounts of soft debris, the effective contact stiffness becomes softer thus reducing the subharmonics. This may also explain why the fit value of tip radius in the model is smaller than expected for this type of cantilever. A smaller tip radius effectively softens the interaction which may mimic the effect of debris on the tip.

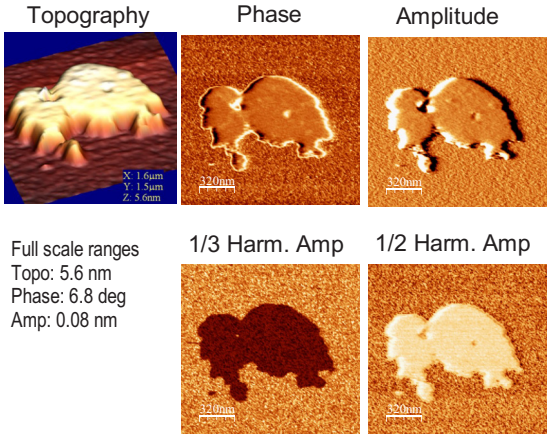

FIG. 3. (Color online) PM on mica, driving frequency just below ω_2. The 1/3 harmonic image appears bright on the mica but dark on the PM, indicating a subharmonic response on the hard substrate but not on the soft sample. $A_{\text{initial}}=4.95$ nm peak, amplitude setpoint=52%, $\Omega_d=78.7$ kHz, $\omega_1=11$ kHz. Image processing by Ref. 22.

The phenomenon of subharmonic response can also be used for mapping compositional contrast. Figure 3 shows images taken of PM on mica with $\Omega_d \approx \omega_2$. In the 1/3 harmonic image, the mica substrate appears bright, whereas the membrane appears dark but the reverse is true for the 1/2 harmonic image. This demonstrates the following result discussed earlier: the operation on the soft PM sample is farther to the right in Fig. 2 than on the hard mica sample. Moving from the hard to soft sample moves the response from a period-3 to a period-2 response.

Finally, subharmonics also have implications in the study of energy dissipation (e.g., on solid-liquid interfaces). To illustrate this, a naive application of the classical tip-sample dissipation formula[20] to the simulated amplitude and phase of Fig. 1 (on mica) would yield the result shown in Fig. 4, which suggests tip-sample dissipation E_{ts} reaches 150 eV/drive cycle. But in fact this simulation uses a conservative model so actually $E_{ts}=0$. Energy is lost from the driving harmonic but instead of transferring to the sample, this energy actually propagates to the first eigenmode (subharmonic response) and to the third eigenmode (momentary excitation[17,21]). To prove this, energy lost to the surrounding

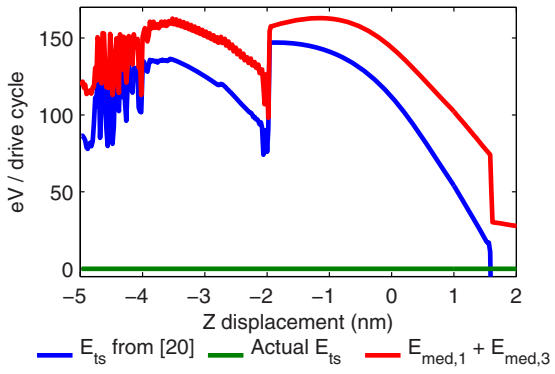

FIG. 4. (Color online) Comparison of energy terms for the simulation in Fig. 1. The classic formula (Ref. 20) predicts a large tip-sample dissipation E_{ts} but the simulation uses a conservative model so actually $E_{ts}=0$. The classic formula is actually predicting the energy that is transferred to other eigenmodes and then dissipated to the fluid media.

viscous fluid by the first and third eigenmode $E_{med,i} = \int_0^T k_i \dot{q}_i^2 / \omega_i Q_i dt$ is also plotted and accounts for nearly all of the classic formula's prediction. Thus the study of tip sample dissipation in liquid environments using the second eigenmode in dAFM needs proper accounting for energy propagation to both lower and higher frequencies.

In conclusion, the operation of dAFM in liquid environments using the second cantilever eigenmode opens up a unique subharmonic energy transfer mechanism to the first eigenmode. This mechanism can offer new opportunities to map compositional contrast but can also challenge the interpretation of conventional energy dissipation spectroscopy. For researchers wanting to avoid subharmonic response while driving the second eigenmode in liquid environments, it is recommended to use stiffer cantilevers (relative to sample stiffness), smaller amplitudes, or preferably cantilevers with overdamped first eigenmodes (e.g., those with short tips).

This research was funded in part by the National Science Foundation through Grant No. CMMI-0927648.

[1]Y. Sugimoto, S. Innami, M. Abe, Ó. Custance, and S. Morita, Appl. Phys. Lett. **91**, 093120 (2007).
[2]R. W. Stark, T. Drobek, and W. M. Heckl, Appl. Phys. Lett. **74**, 3296 (1999).
[3]X. Xu and A. Raman, J. Appl. Phys. **102**, 034303 (2007).
[4]T. R. Rodríguez and R. García, Appl. Phys. Lett. **84**, 449 (2004).
[5]J. Melcher, S. Hu, and A. Raman, Rev. Sci. Instrum. **79**, 061301 (2008).
[6]S. Basak and A. Raman, Appl. Phys. Lett. **91**, 064107 (2007).
[7]E. Herruzo and R. García, Appl. Phys. Lett. **91**, 143113 (2007).
[8]R. García and A. San Paulo, Phys. Rev. B **60**, 4961 (1999).
[9]N. A. Burnham, A. J. Kulik, G. Gremaud, and G. A. D. Briggs, Phys. Rev. Lett. **74**, 5092 (1995).
[10]S. Salapaka, M. Dahleh, and I. Mezić, Nonlinear Dyn. **24**, 333 (2001).
[11]W. van de Water and J. Molenaar, Nanotechnology **11**, 192 (2000).
[12]S. Hu and A. Raman, Phys. Rev. Lett. **96**, 036107 (2006).
[13]F. Jamitzky, M. Stark, W. Bunk, W. M. Heckl, and R. W. Stark, Nanotechnology **17**, S213 (2006).
[14]R. W. Stark, Nanotechnology **15**, 347 (2004).
[15]A. Dick, B. Balachandran, H. Yabuno, M. Numatsu, K. Hayashi, M. Kuroda, and K. Ashida, J. Comput. Nonlinear Dyn. **5**, 1 (2009).
[16]S. Rützel, S. Lee, and A. Raman, Proc. R. Soc. London, Ser. A **459**, 1925 (2003).
[17]J. Melcher, C. Carrasco, X. Xu, J. L. Carrascosa, J. Gómez-Herrero, P. J. D. Pablo, and A. Raman, Proc. Natl. Acad. Sci. U.S.A. **106**, 13655 (2009).
[18]S. W. Shaw and P. J. Holmes, J. Sound Vib. **90**, 129 (1983).
[19]R. C. Tung, A. Jana, and A. Raman, J. Appl. Phys. **104**, 114905 (2008).
[20]B. Anczykowski, B. Gotsmann, H. Fuchs, J. P. Cleveland, and V. B. Elings, Appl. Surf. Sci. **140**, 376 (1999).
[21]D. Martínez-Martín, C. Carrasco, D. Kiracofe, J. Melcher, R. Pérez, M. Mateu, J. Carrascosa, A. Raman, P. de Pablo, and J. Gómez-Herrero (unpublished).
[22]I. Horcas, R. Fernandez, J. Gomez-Rodriguez, J. Colchero, J. Gomez-Herrero, and A. M. Baro, Rev. Sci. Instrum. **78**, 013705 (2007).
[23]Experiments were also performed with magnetic drive but the second eigenmode was hard to excite sufficiently thus subharmonics could not be seen as well compared to acoustic drive.
[24]At least two eigenmodes are needed to predict dynamics when driving the first eigenmode in liquids.[6] We found three eigenmodes necessary while driving the second eigenmode.
[25]Under conditions relevant to typical biological AFM (high concentration buffer solutions with amplitudes $>2-3$ nm) the forces due to adhesion, the electrical double layer, and solvation shells are relatively small and have little effect on the dynamics, justifying the use of Hertz model as opposed to more detailed models.
[26]The experimental time history was acquired in a separate measurement from the approach curves. Time history was acquired at a steady-state Z to reduce noise and comb filtered to multiples of $\Omega_d/4$ with a 1 kHz bandwidth.